Environmental Modelling and Software 204 (2026) 107082

Contents lists available at ScienceDirect

Environmental Modelling and Software

journal homepage: www.elsevier.com/locate/envsoft

Composite2Change (C2C) on Google Earth Engine: Time-series change detection and metrics characterizing disturbance and recovery

Txomin Hermosilla [a,*], Michael A. Wulder [a], Joanne C. White [a], Nicholas C. Coops [b], Daniel Coelho [c], Giovanni Ciatto [d], Noel Gorelick [e], Emma Bambagioni [f], Saverio Francini [f]

[a] Canadian Forest Service (Pacific Forestry Centre), Natural Resources Canada, 506 West Burnside Road, Victoria, British Columbia, V8Z 1M5, Canada
[b] Integrated Remote Sensing Studio, Department of Forest Resources Management, University of British Columbia, 2424 Main Mall, Vancouver, BC, V6T 1Z4, Canada
[c] Google, 1600 Amphitheatre Parkway, Mountain View, CA, 94043, USA
[d] Department of Computer Science and Engineering, Alma Mater Studiorum-Università di Bologna, Via dell'Università 50, Cesena, Emilia-Romagna, 47522, Italy
[e] Cantrip AG, Switzerland
[f] Department of Science and Technology of Agriculture and Environment (DISTAL), University of Bologna, Bologna, 40126, Italy

A R T I C L E I N F O

Keywords:
Disturbance monitoring
Forest dynamics
Landsat
Sentinel-2
Land cover
Change metrics
Cloud computing

A B S T R A C T

Satellite time series enable the consistent and scalable characterization of land cover changes and vegetation dynamics across extensive areas. The Composite2Change (C2C) protocol applies temporal spectral trend analysis to identify land change events, producing metrics that describe the timing, magnitude, duration, rate, direction, and recovery dynamics of disturbances. These metrics summarize spectral trajectories and support mapping and modelling applications. While the methods have been published and their value demonstrated, their replication across regions and sensors has been limited due to high storage and computational demands, coupled with the lack of available implementation. To address these barriers, we implemented C2C as a reproducible cloud-native framework within Google Earth Engine (C2C-GEE). C2C-GEE enables users to generate change products and metrics that describe the spectral and temporal signatures of land cover change and recovery. The framework supports the transparent and systematic generation of standardized change metrics for large-area mapping and modelling applications worldwide.

1. Introduction

Free and open access to satellite imagery in increasingly analysis-ready formats, combined with high-performance computing (Wulder and Coops, 2014), has resulted in a proliferation of methods for characterizing and mapping terrestrial vegetation dynamics (Cohen et al., 2017; Hughes et al., 2017). Approaches for analyzing large volumes of satellite data over space and time have been widely adopted (Griffiths et al., 2013; Hermosilla et al., 2024a; White et al., 2014), often prototyped and implemented on clusters of high-performance computers (Chen et al., 2012). These refined, tested, and published approaches are increasingly being shared via cloud computing platforms such as Google Earth Engine (GEE) (Gorelick et al., 2017), which enables users to access data and processing capabilities while reducing the need for local infrastructure to download, store, and process data. Such a paradigm allows users to bring their algorithms to the data, rather than the less efficient but more common requirement of bringing their data to the algorithms.

Image compositing and change detection approaches are integral to enabling the monitoring of forest dynamics over very large forest areas. Image compositing approaches have been developed to generate cloud-free, radiometrically consistent image composites that combine multiple medium-resolution optical observations over large areas (Francini et al., 2023), ranging from regional (Griffiths et al., 2014; Hermosilla et al., 2015a; Roy et al., 2010) to global scales (Hansen et al., 2013). Similarly, the development of various time-series analysis algorithms has enabled the detection and characterization of vegetation trends and changes (DeVries et al., 2015a; Griffiths et al., 2014; Kennedy et al., 2012; Verbesselt et al., 2010; White et al., 2017). The information requirements of a given application should guide the selection of the appropriate compositing window (White et al., 2014) and inform the development or selection of a specific change detection approach, as

* Corresponding author.
E-mail address: txomin.hermosillagomez@nrcan-rncan.gc.ca (T. Hermosilla).

https://doi.org/10.1016/j.envsoft.2026.107082
Received 4 March 2026; Received in revised form 3 June 2026; Accepted 16 June 2026
Available online 19 June 2026

different change detection methods produce different results (Cohen et al., 2017). Ultimately, the changes identified reflect the compositing window selected, the image data used and its associated spectral characteristics, the time step between images, the algorithm applied, and other methodological considerations (Hughes et al., 2017; Zhu, 2017). Ensemble approaches also create opportunities to combine outputs from multiple change detection algorithms and refine results to better target particular disturbance types (Cohen et al., 2020; Healey et al., 2018; Schroeder et al., 2014).

Multi-year time series analyses provide a detailed characterization of forest change dynamics and offer additional insights into the nature of change processes (Comber and Wulder, 2019). Abrupt, punctual changes such as severe forest fires or clear-cut harvesting, are relatively straightforward to capture and have historically been detected using two images acquired at different times (Hansen and Loveland, 2012; Woodcock et al., 2020). In contrast, gradual, non-punctual changes such as insect infestation or water stress are manifested over periods measured in years (Coops et al., 2020; Vogelmann et al., 2012, 2016). Time-series approaches can detect both abrupt and gradual changes, generating descriptive metrics that are valuable for distinguishing between different drivers and types of change (Hermosilla et al., 2015a; Kennedy et al., 2012). Processing time series of spatially and radiometrically consistent imagery provides a means of capturing and condensing information on change dynamics across space and time (Zhu, 2017). Descriptors of change summarize time series trends, providing rich yet manageable insights into complex dynamics at the pixel level. Examples of change descriptors that can be extracted from a spectral time series are magnitude, rate, duration, and directionality (Chirici et al., 2020; White et al., 2018). Such metrics enable consistent, spatially explicit assessments of post-disturbance dynamics and support the quantification of vegetation and forest return following disturbance. Spectral change metrics relating forest recovery, for instance, can be used to identify areas of delayed recovery and inform management and reporting needs (White, 2024). These metrics describing the nature of change dynamics can improve biophysical models (Pflugmacher et al., 2014), disturbance agent classification (Stahl et al., 2023), and the identification and classification of non-punctual changes (Coops et al., 2020).

Google Earth Engine (GEE) is a cloud-based geospatial analysis platform that provides high-performance computing resources and access to geospatial datasets and Earth observation imagery, including the complete Landsat and Sentinel-2 archives (Gorelick et al., 2017). While many GEE workflows are implemented through user-defined scripts, native platform functions operate within the underlying computational infrastructure, supporting efficient processing of computationally intensive procedures such as time series analysis and breakpoint detection. Well-established native change detection functions available in GEE include LandTrendr (Kennedy et al., 2018), BFAST (Hamunyela et al., 2020), and CCDC (Arévalo et al., 2020). While these approaches offer well-documented methodologies and interpretable results, they do not natively provide a unified set of standardized, operational metrics for measuring vegetation disturbance and recovery.

The Composite2Change (C2C) protocol generates spatially explicit metrics describing change and post-disturbance recovery by applying temporal spectral trend analysis to radiometrically consistent, cloud-free image composites (Hermosilla et al., 2016). These metrics quantify change magnitude, duration, and post-disturbance dynamics, spectrally characterizing vegetation recovery (Hermosilla et al., 2015a, 2015b; White et al., 2017, 2019). They also support operational forest monitoring initiatives, including those within Canada's National Forest Inventory and carbon accounting frameworks (e.g., Baral et al., 2025; Smyth et al., 2024). While C2C was initially developed for application with Landsat surface reflectance data, the protocol's conceptual framework can be adapted to different compositing strategies and optical satellite data sources, including Sentinel-2 and Harmonized Landsat Sentinel-2 (HLS). To date, large-area and long-term applications of C2C have required local data storage and high-performance computing resources, which have motivated the development of a scalable implementation within the GEE cloud-computing environment.

This study presents a scalable and reproducible implementation of the C2C protocol in GEE. The algorithmic framework (hereafter C2C-GEE) is written as native Java functions within the GEE backend to support efficient large-area processing. C2C-GEE enables the generation of temporally explicit, standardized change and recovery metrics suitable for a wide range of information needs. These metrics include change timing, descriptors of change dynamics (e.g., magnitude, duration, and rate), and spectral recovery metrics characterizing post-disturbance regrowth. The resulting outputs are designed for direct use in large-area monitoring, comparative analyses, and downstream modelling applications, and can be accessed within the GEE environment or exported for further analysis.

2. Methods

2.1. C2C protocol overview

The Composite2Change (C2C) protocol (Hermosilla et al., 2016) enables the detection and characterization of changes using free and open optical data from the Landsat and Sentinel-2 archives. Annual composites are typically generated using a best-available-pixel (BAP) method (Griffiths et al., 2013; White et al., 2014), in which optimal pixel observations are selected from all available surface-reflectance imagery (Masek et al., 2006; Schmidt et al., 2013). Other compositing strategies (e.g., medoid compositing) may also be employed depending on the analysis objectives (Francini et al., 2023; Meng et al., 2023; Qiu et al., 2023).

The overall C2C workflow can be summarized in four main stages: (1) generation of temporally consistent annual image composites, (2) temporal noise filtering and spike handling, (3) temporal segmentation and breakpoint detection using bottom-up piecewise fitting, and (4) extraction of disturbance and recovery metrics from the spectral trajectories (see Fig. 1).

The annual image composites are analyzed in the time domain to reduce residual noise arising from unscreened atmospheric effects (e.g., haze, clouds, cloud shadows, smoke) and to ensure temporal consistency prior to change detection (Hermosilla et al., 2015a). Noisy observations can be identified and removed by evaluating temporal inconsistencies across consecutive years and multiple spectral bands (Kennedy et al., 2010). Observations identified as noise are excluded from the subsequent analysis, improving the robustness of the temporal segmentation and change characterization.

Temporal trend and change analysis in C2C is performed using an adapted bottom-up breakpoint detection algorithm (Keogh et al., 2001). This approach involves the iterative merging of adjacent temporal segments based on a root mean square error (RMSE) criterion until either the maximum user-defined fitting error is reached or the maximum number of segments is exceeded. More restrictive merging costs tend to identify changes of a greater magnitude, but they may not fully represent the spatial extent of the change event. In contrast, less restrictive merging costs provide more comprehensive characterizations of change, increasing sensitivity to lower-magnitude disturbances and vegetation responses, and potentially leading to an increased occurrence of false positives (Fig. 2). This process results in the identification of temporal segments and associated trends, which are then used to identify changes and generate a set of metrics that characterize the nature of the changes (i.e., magnitude, duration, and rate), as well as pre- and post-disturbance dynamics associated with vegetation recovery following disturbances. The Normalized Burn Ratio (NBR; Key and Benson, 2006) is the vegetation index typically employed for temporal and change analysis within the C2C protocol although other indices may be selected (Hermosilla et al., 2016).

In the original C2C workflow, temporal trends derived from

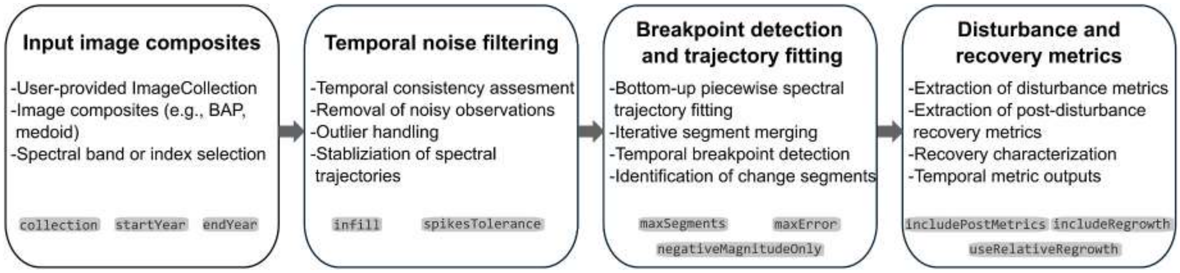

Fig. 1. Overview of the Composite2Change (C2C) workflow and the main parameters associated with each processing stage as parameterized in C2C-GEE (see Table 1).

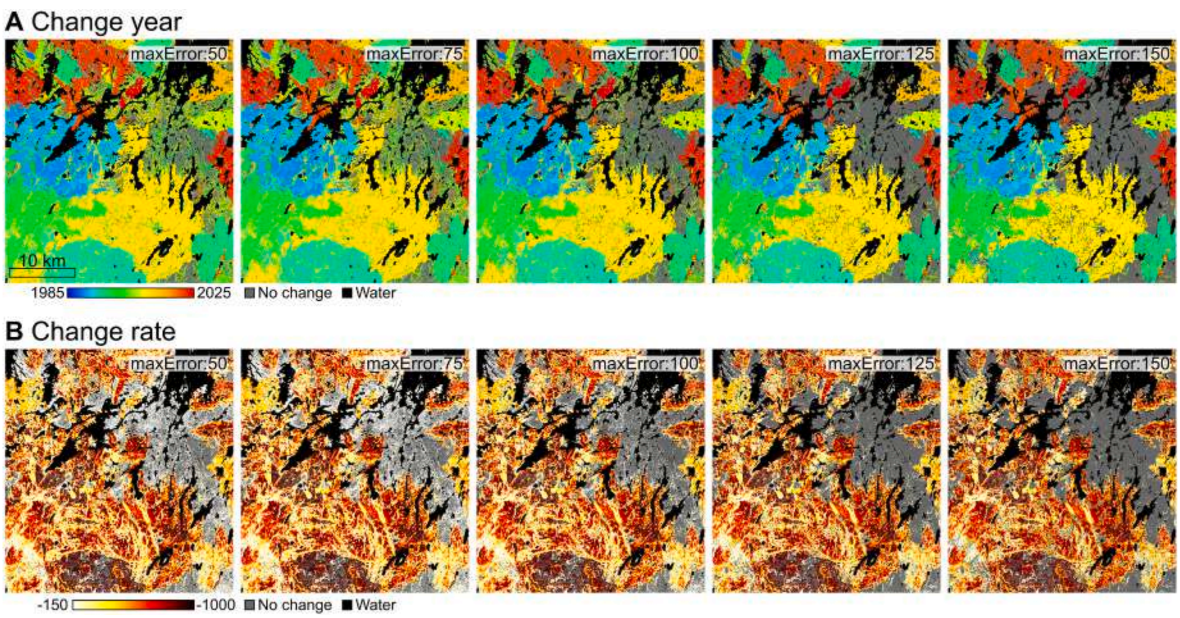

Fig. 2. Example of the effect of the root mean square error (RMSE) criterion controlled by the `maxError` parameter on C2C-GEE outputs (Table 1), showing (A) change year and (B) change rate derived from annual Landsat composites of the Normalized Burn Ratio (NBR) index for the period 1984-2025 using Best Available Pixel (BAP) compositing in Canada (lat: 56.137, lon:-102.161). Disturbance events with a NBR magnitude ≤ -200 (NBR $\times$ 1000) were retained. Values above/below the upper/lower limits of the portrayed change rate range are truncated.

segmentation support gap filling through piecewise linear interpolation, to produce gap-free annual best available pixel (BAP) composite products (Hermosilla et al., 2015a). In the GEE implementation of C2C, annual image composites are assumed to be provided as inputs using user-defined or existing compositing tools in GEE. Tools such as GEE-BAP (Francini, 2022) provide similar BAP compositing functionality to that described in (Griffiths et al., 2013; White et al., 2014) without the gap filling capability of (Hermosilla et al., 2015a). Thus, C2C-GEE focuses exclusively on change detection and metric extraction.

2.2. C2C implementation in Google Earth Engine

C2C-GEE implements the temporal segmentation and change metric extraction components of the C2C protocol as a native Earth Engine algorithm running on the server. By embedding these procedures within the GEE backend, the need for user-managed data storage and local processing workflows is eliminated, enabling scalable execution of the iterative segmentation routines required by C2C. The GEE implementation follows the original C2C algorithmic design and parameterization to ensure consistency in breakpoint detection and metric derivation. Processing occurs within the Earth Engine computational environment, supporting large-area analyses without data transfer overhead and standardizing execution across users and applications. The function can be accessed via the GEE API (ee.Algorithms.TemporalSegmentation.C2c) and invoked from JavaScript or Python clients.

The C2C-GEE function takes an ImageCollection representing a temporally ordered sequence of images (typically annual image composites) as input, along with one or more spectral bands or indices (e.g. NBR). User interaction is limited to specifying the input data and a defined set of parameters that control different stages of the workflow, including segmentation sensitivity, model complexity, the temporal extent, and the optional computation of post-change and recovery metrics (Table 1). Segmentation behaviour is primarily governed by the maximum allowable root mean squared error (`maxError`) and the maximum number of permitted segments (`maxSegments`). Additional options support robustness to residual artifacts and data gaps, including optional gap infilling (`infill`) for segmentation stability, and tolerance to spectral spikes or outliers (`spikesTolerance`). There is no explicit limit on the number of consecutive missing observations during the gap infilling; however, confidence in the fitted temporal trajectory decreases as this number increases (Hermosilla et al., 2015a). These tolerances were originally included to accommodate earlier periods of the Landsat archive (mid-1980s to early 2000s), when image availability was more limited in terms of space and time (Wulder et al., 2016). However, given the current availability of Landsat and Sentinel-2 observations, the need for gap filling is less common and is now more typically associated with persistent cloud, smoke, or haze conditions (Ju et al., 2025).

Table 1
Parameters used in the C2C-GEE implementation, with descriptions and default values.

Parameter	Default value	Description and role
`collection`	-	Input `ImageCollection` time series (e.g., annual composites or spectral index trajectories) with valid timestamps.
`dateFormat`	0	Time encoding for outputs: 0 = Julian days, 1 = fractional years, 2 = Unix milliseconds.
`maxError`	75	Maximum allowed RMSE of the piecewise linear fit, controlling segmentation sensitivity.
`maxSegments`	6	Maximum number of segments permitted in the fitted trajectory.
`startYear`	1984	First year of the analysis period.
`endYear`	2025	Last year of the analysis period.
`infill`	true	Enables gap infilling within the time series to support stable fitting in the presence of missing values.
`spikesTolerance`	0.85	Controls tolerance to short-lived spikes/outliers in the trajectory.
`includePostMetrics`	true	Returns post-change descriptors (`postMagnitude`, `postDuration`, `postRate`).
`includeRegrowth`	false	Returns recovery and regrowth metrics (`indexRegrowth`, `recoveryIndicator`, `regrowth60/80/100`).
`useRelativeRegrowth`	false	Computes regrowth thresholds relative to pre-disturbance conditions.
`negativeMagnitudeOnly`	false	Retains only breakpoints associated with negative changes.

Table 2
Output metrics generated by the C2C-GEE implementation. Outputs are returned as array-valued images aligned to the fitted temporal segment structure. See Fig. 3 for graphical representation of selected metrics.

Output metric	Description	Citation
`changeDate`	Start and end dates for each fitted temporal segment, encoded according to the dateFormat parameter.	(Hermosilla et al., 2015a, 2016; Keogh et al., 2001)
`value`	Fitted values of the input band evaluated at the dates defined by changeDate.	(Hermosilla et al., 2015a, 2016)
`magnitude`	Absolute difference between fitted values before and after each change date, representing change magnitude. The first element is NaN.	(Hermosilla et al., 2016; Kennedy et al., 2010)
`duration`	Duration of the temporal segment preceding each change date. The first element is NaN.	(Hermosilla et al., 2015a; White et al., 2017)
`rate`	Rate of change of the temporal segment preceding each change date, derived from the fitted trajectory. The first element is NaN.	(Hermosilla et al., 2016; Kennedy et al., 2010)
`postMagnitude`	Magnitude of the temporal segment following each change date. The last element is NaN.	Hermosilla et al. (2016)
`postDuration`	Duration of the temporal segment following each change date. The last element is always NaN.	Hermosilla et al. (2016)
`postRate`	Rate of change of the temporal segment following each change date, characterizing post-change trends. The last element is NaN.	Hermosilla et al. (2016)
`indexRegrowth`	Absolute difference between the fitted value at the change date and the fitted value five data points after the change date, representing short-term post-disturbance regrowth.	Kennedy et al. (2012)
`recoveryIndicator`	Ratio of indexRegrowth to magnitude, providing a relative measure of recovery normalized by disturbance magnitude.	(Kennedy et al., 2012; White et al., 2017)
`regrowth60`	Time elapsed between the change date and the first point at which the fitted series reaches 60% of the pre-disturbance value. Also referred to as Years to Recovery metric.	(Pickell et al., 2016; White et al., 2018)
`regrowth80`	Time elapsed between the change date and the first point at which the fitted series reaches 80% of the pre-disturbance value. Also referred to as Years to Recovery metric.	(Pickell et al., 2016; White et al., 2018)
`regrowth100`	Time elapsed between the change date and the first point at which the fitted series reaches 100% of the pre-disturbance value. Also referred to as Years to Recovery metric.	(Pickell et al., 2016; White et al., 2018)

Temporal controls define the analysis period and the encoding of date-related outputs. The analysis period is constrained using `startYear` and `endYear`, in addition to any temporal filtering applied directly to the input `ImageCollection`. Output time encoding is controlled by `dateFormat`, which specifies whether dates are returned as Julian days, fractional years, or Unix time (milliseconds); all date and time-difference outputs (e.g. segment length) are reported in the corresponding units.

Disturbance characterization outputs are returned as array-valued images, allowing multiple temporal segments and change events to be represented per pixel (Table 2, Fig. 3). For each analyzed band, C2C-GEE returns arrays describing segment timing (`changeDate`), fitted values (`value`), and breakpoint-linked change metrics, including `magnitude`, `duration`, and `rate`. Optional post-change descriptors (`postMagnitude`, `postDuration`, `postRate`) characterize the dynamics of the segment following each breakpoint. By convention, the first element of pre-change metric arrays and the last element of post-change metric arrays are undefined (NaN). For applications requiring a single disturbance event (e.g. disturbance mapping), these arrays can be post-processed to extract an event of interest, such as the breakpoint with the greatest negative magnitude. Directional filtering can be applied using `negativeMagnitudeOnly` to retain only breakpoints associated with negative changes in the input series. Note that any negative segment identified in the fitted trajectory represents a detected spectral change. In practice, users may further apply additional change magnitude or rate thresholds, such as a minimum NBR change magnitude, to focus on changes associated with stronger vegetation responses.

Recovery and regrowth metrics are returned when `includeRegrowth = true` is set. These include short-term regrowth (`indexRegrowth`), a normalized recovery indicator (`recoveryIndicator`) and the time taken to reach 60%, 80% and 100% recovery (`regrowth60`, `regrowth80` and `regrowth100`). Two alternative formulations are available for computing recovery levels (60%, 80% and 100%), controlled by the `useRelativeRegrowth` parameter. When `useRelativeRegrowth` is set to `false` (the default setting), recovery is evaluated relative to pre-disturbance fitted values, which is consistent with previous Landsat time-series recovery approaches. When `useRelativeRegrowth = true` is set, recovery is expressed as the fraction of disturbance magnitude that has been regained, providing a normalized measure that reduces dependence on the absolute scale of the input spectral index. The `useRelativeRegrowth` option enables recovery to be expressed as a fraction of disturbance magnitude, normalizing recovery estimates across index scales and disturbance intensities. The `indexRegrowth` recovery metric is only computed where at least five

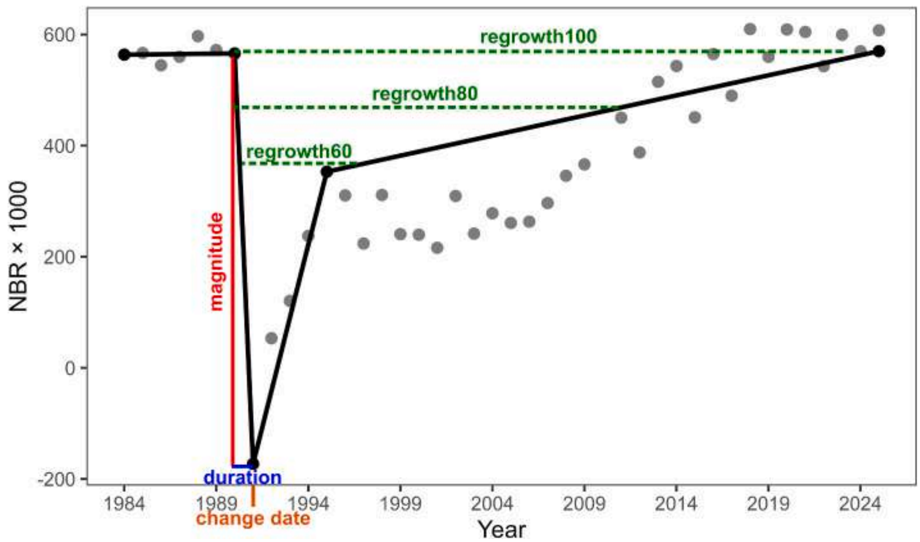

Fig. 3. Schematic representation of disturbance and recovery metrics derived from a negative spectral change segment. Dots represent annual NBR observations (×1000), and solid lines indicate fitted temporal segments. The disturbance event occurs between 1989 and 1990. Magnitude, duration, change date, and post-disturbance recovery thresholds at 60%, 80% and 100% (regrowth60, regrowth80, regrowth100) are shown. See Table 2 for complete definitions of all output metrics.

post-disturbance observations exist following the detected change event. Global (Fig. 4) and regional examples in Canada (Fig. 5A) and France (Fig. 5B) illustrate disturbance and recovery metrics using C2C-GEE.

The consistency between the two implementations was assessed by comparing outputs generated by the C2C-GEE implementation with those produced by the standard local C2C framework (Hermosilla et al., 2015a) across a set of test sites distributed throughout the northern hemisphere (Figure A1). Results showed high consistency between implementations in annual disturbance detections and in the distributions of disturbance magnitude (r = 0.99, RMSE = 3.03%, bias = 0.13%) and recovery indicator values (r = 0.91; RMSE = 14.05%, bias = 0%).

3. Discussion

3.1. Scope and design of the C2C-GEE implementation

The C2C-GEE implementation operationalizes the temporal segmentation and change metric extraction components of the C2C protocol (Hermosilla et al., 2016) within the GEE environment (Gorelick et al., 2017). The GEE implementation presented here focuses explicitly on change detection and the derivation of disturbance and recovery metrics for terrestrial vegetation from temporally consistent, image composites supplied by the user. This design simplifies the workflow and enhances flexibility by allowing input composites to be generated using existing or user-defined compositing approaches available in GEE, tailored to specific monitoring objectives and data availability (White et al., 2014). As a result, C2C-GEE can be readily integrated into a wide range of analysis pipelines without enforcing a fixed compositing strategy or seasonal window. This separation preserves flexibility in compositing and maintains a standardized framework for extracting change metrics. The C2C-GEE implementation facilitates the scalable processing of large Earth observation archives without the need for local high-performance computing infrastructure, while enabling the direct integration of other datasets and workflows available on GEE. However, execution times and processing limitations remain subject to the platform's computational constraints and task management policies, particularly when processing dense time series observations over large spatial extents.

Data products with annual time stamps are typically required for forest monitoring and modelling applications (White et al., 2014) and therefore commonly used as inputs to C2C-GEE. Annual composites help to ensure sufficient observational coverage despite the uneven spatial and temporal distribution of images in the archive, especially during earlier periods (Wulder et al., 2016). Previous applications of C2C have relied on annual summer composites and the NBR to characterize forest disturbance and recovery dynamics across boreal and temperate forest environments (Hermosilla et al., 2015b, 2016; Tortini et al., 2019; White et al., 2018, 2022). The summer seasonal window captures the vegetation growing season and maximizes the availability of cloud-free observations (White and Wulder, 2014), although the specific date range should be defined based on latitude and monitoring objectives.

NBR is sensitive to changes in forest structure (Cohen and Goward, 2004) and has demonstrated strong performance for monitoring forest dynamics (Cohen et al., 2018). Using C2C in non-boreal environments may require alternative spectral indices and parameter settings. The default parameter values provided in C2C-GEE are based on previous applications of the C2C methodology and have demonstrated reliable performance across a range of forest environments and disturbance conditions (Matasci et al., 2018; Tortini et al., 2019; White et al., 2018). However, the selection of optimal parameters remains dependent on the application and should be adapted according to the study area, disturbance characteristics, spectral inputs, and particular monitoring objectives. To accommodate differences in local vegetation dynamics and image availability, C2C-GEE enables the simultaneous evaluation of multiple spectral indices and alternative segmentation parameter settings. This allows users to customize disturbance detection and recovery characterization according to local ecological conditions, facilitating integration into forest monitoring frameworks operating under varying environmental and data constraints. C2C-GEE performance depends on the quality of input composites and segmentation parameter selection, while the compact parameter set and standardized outputs support reproducible reprocessing and sensitivity analyses.

3.2. Change metrics

Using free and open data from the Landsat, Sentinel-2, and potentially other satellite missions, C2C-GEE produces a set of spectral and temporal metrics that describe the detected changes and their dynamics from multiple perspectives (Zhu et al., 2022). These include the magnitude and duration of the change, as well as the spectral trends describing the vegetation condition before and after the disturbance. Greater change magnitudes are typically associated with more severe disturbance agents (DeVries et al., 2015b), while change duration

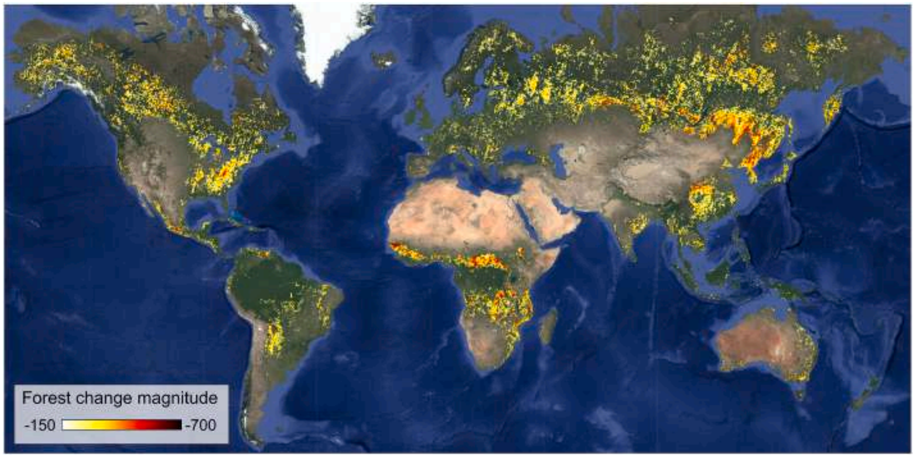

Fig. 4. Global map of change magnitude detected from a 500-m spatial resolution, global Landsat medoid composites of the Normalized Burn Ratio index for the period 1984-2025.

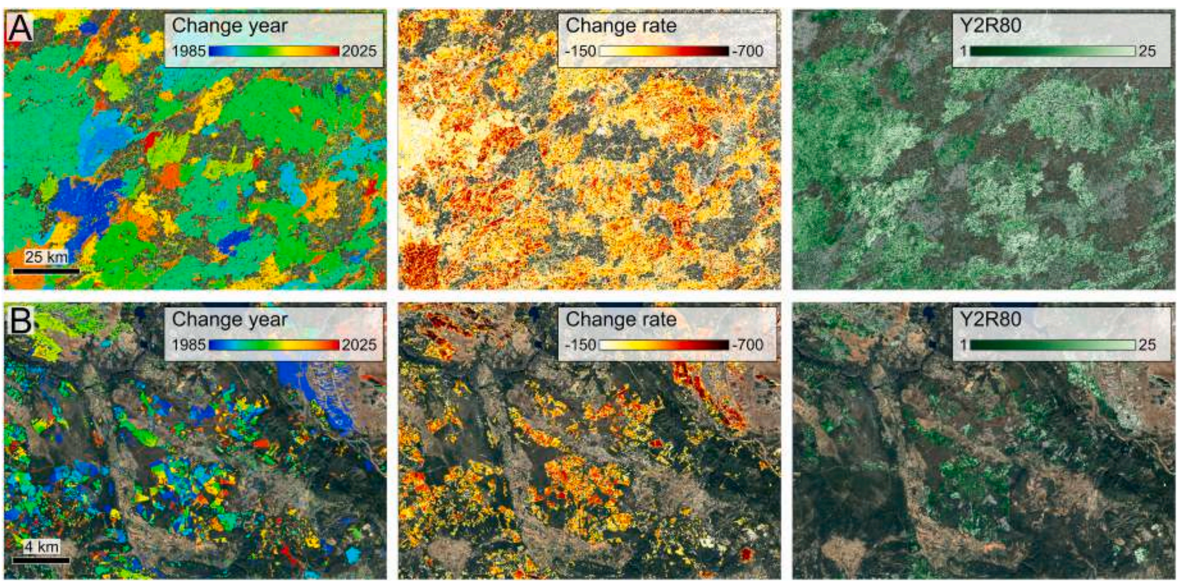

Fig. 5. Regional examples of forest disturbance metrics derived from annual Landsat composites of the Normalized Burn Ratio (NBR) index for the period 1984-2025, including (A) Canada (lat: 61.1360, lon:-108.0649), using Best Available Pixel (BAP) compositing, and (B) France (lat: 43.6218, lon: 6.1439), using medoid compositing, displaying change year, change rate, and years to recovery at 80% (Y2R80) metrics. Disturbance events with a NBR magnitude ≤ -200 (NBR $\times$ 1000) were retained. Values above/below the upper/lower limits of the portrayed change rate range are truncated.

captures the persistence of the event. Rapid changes often correspond to stand-replacing disturbances (e.g., harvest, wildfire), while more gradual processes (e.g., water stress, insect defoliation) manifest over longer periods of time (Coops et al., 2006). Furthermore, the duration metric also allows differentiation between gradual processes driven by different disturbance agents, such as insect disturbance causing defoliation and tree mortality (Meigs et al., 2011; Senf et al., 2017). Pre-disturbance values provide additional context by capturing baseline vegetation conditions and trajectories (i.e., growth, decline) prior to the occurrence of disturbance (Coops et al., 2020; Hais et al., 2016).

Change metrics are spatially explicit and can be mapped directly or used as input layers in modelling applications. Examples include habitat (Kearney et al., 2019) and species movement analyses (Rickbeil et al., 2017), fire severity (Mulverhill et al., 2024; Shang et al., 2020), insect outbreak risk predictions (Hais et al., 2016), land cover stabilization (Hermosilla et al., 2018), tree species transitions (Hermosilla et al., 2024b), and characterization of forest structure, including overstory (Matasci et al., 2018; Pflugmacher et al., 2014) and understory conditions (Vogeler et al., 2016). While C2C has typically been used to monitor vegetation, other spectral indices can be applied to track different aspects of land dynamics. For example, indices related to land imperviousness (e.g. Normalized Difference Built-up index; Zha et al., 2003) allow analysis of the magnitude, timing, and duration of urban expansion processes (Fu et al., 2019; Song et al., 2016).

The spatio-temporal characteristics of change can also support attribution to a disturbance agent (Stahl et al., 2023). This process often requires moving from a pixel-level to an object-level approach by grouping adjacent pixels that have experienced change in the same year (Stewart et al., 2009). These change events can then be spectrally characterized using summary statistics (e.g., mean, standard deviation, median, percentiles) from change metrics (e.g., magnitude, rate), descriptors of pre- and post-change trends, full-time series descriptors (Hermosilla et al., 2015b), and additional ancillary data such as topography or climate (Schroeder et al., 2017). Added informational value can be gained by describing object-based change events using their geometric properties, including size, shape and complexity (Hilker, 2011; Sebald et al., 2021), which, when combined with spectral-temporal change metrics, support supervised, rule-based, or unsupervised discrimination of disturbance agents (Hermosilla et al., 2016; Kennedy et al., 2015; Pickell et al., 2014; Pouliot and Latifovic, 2016; Shimizu et al., 2017; Vogeler et al., 2020; Zhang et al., 2022). Additionally, change metrics can aid in distinguishing typologies within the same agent, including different forest harvesting practices (Esteban et al., 2021; Giambelluca et al., 2025; Jarron et al., 2017), fires by severity (Schleeweis et al., 2020), as well as insect infestations (Pasquarella et al., 2021; Senf et al., 2015; Thapa et al., 2022; Ye et al., 2021b) and other drivers of non-stand replacing disturbances (Brown et al., 2025; Coops et al., 2020).

3.3. Recovery metrics

The C2C-GEE implementation provides a scalable framework for the consistent characterization of post-disturbance dynamics and recovery trajectories across large spatial extents by operationalizing the extraction of disturbance and recovery metrics from satellite time series. It supports standardized recovery assessments across regions and disturbance contexts, eliminating the need for custom post-processing workflows. Post-disturbance spectral trends provide a basis for measuring and monitoring vegetation recovery over time (Frolking et al., 2009). Within C2C-GEE, recovery is quantified by tracking the temporal trajectory of spectral indices after a disturbance breakpoint. This involves estimating the rate and magnitude of return to pre-disturbance conditions and deriving metrics such as scaled recovery indicators and years-to-recovery thresholds. Landsat time series offer two key advantages for assessing forest recovery: they provide consistent annual or semi-annual observations, and they support retrospective analyses that allow the characterization of pre-disturbance conditions and the establishment of recovery baselines (Potapov et al., 2015; White et al., 2017). Spectral recovery metrics can also be integrated with other data sources, such as Airborne Laser Scanning (ALS) and field plots, to provide a comprehensive framework for characterizing recovery trajectories (Bolton et al., 2015; Smith-Tripp et al., 2026; White et al., 2018) or to improve the prediction of ecosystems variables such as carbon storage (Francini et al., 2025). Given that slow forest recovery has implications for sustainable forest management and policy (Frolking et al., 2009; Pugh et al., 2019), there is a growing need for spatially explicit recovery monitoring based on consistent data sources over large areas (White, 2024). Spectral recovery metrics are useful for estimating and comparing regrowth rates across space and time (White et al., 2017; Frazier et al., 2018; Senf and Seidl, 2022), and for quantifying recovery performance under varying conditions, including disturbance severity (White et al., 2022), vegetation type (Bright et al., 2019), and the presence of previous disturbance (Hermosilla et al., 2019; Mandl et al., 2025).

Clear and measurable definitions of forest recovery are essential precursors to spectral recovery assessments (White, 2024). Applications using C2C have typically defined forest recovery as the return of trees capable of reaching >5 m height and >10% canopy cover (e.g. White et al., 2022). However, definitions of recovery vary depending on the objectives of the assessment (e.g., silviculture, habitat, reclamation) and may relate to the return of forest structure, composition, function, or a combination thereof (e.g. Kearney et al., 2019).

A variety of spectral indices have been employed to assess post-disturbance recovery, reflecting differences in sensitivity to vegetation structure and composition (Chu and Guo, 2013; Mandl et al., 2025; White, 2024). Normalized Difference Vegetation Index (NDVI) tends to saturate rapidly upon the return of herbaceous cover. In contrast, NBR exploits the differing near infrared and shortwave infrared responses associated with bare ground and forest canopy development. This makes NBR more sensitive to the re-establishment of trees and the increasing complexity of canopy (Pickell et al., 2016). Other approaches have proposed alternative indices (Chu et al., 2017) or used ensembles of multiple indices to characterize recovery dynamics (Smith-Tripp et al., 2024). Historically, recovery assessments within the C2C framework were based on trend-fitted NBR values (White et al., 2017), using a de-spiking approach (Hermosilla et al., 2015a) to reduce interannual variability in the spectral response (Schroeder et al., 2007). Ultimately, the choice of index must be consistent with the definition of recovery applied (White, 2024).

C2C-GEE provides a suite of spectral recovery metrics that capture both short-term (Kennedy et al., 2012) and long-term (Griffiths et al., 2014; Pickell et al., 2016) post-disturbance recovery (Table 2). Studies have recommended the use of both short-term and long-term recovery metrics to capture different aspects of recovery (Chu and Guo, 2013; Kennedy et al., 2012). Others have investigated whether short-term metrics are indicative of long-term recovery outcomes (Smith-Tripp et al., 2025; White et al., 2022). The recovery indicator (Table 2), which scales the index regrowth by the magnitude of change, takes into account areas that were sparsely vegetated prior to disturbance or experienced low-intensity disturbance, where more remnant vegetation remained (Kennedy et al., 2012). Hermosilla et al. (2019) and White et al. (2017) used the recovery indicator to assess short-term recovery rates across Canada following stand-replacing wildfire and harvest (i.e. salvage harvest). Hermosilla et al., 2019 also compared the recovery indicator in areas affected by a single disturbance to those areas that experienced two or more disturbances and found that recovery was 39% slower when harvest followed wildfire compared to recovery rates following a single wildfire event.

The Years to Recovery (Y2R) metric transforms the NBR time series into a recovery indicator by estimating the number of years required for a pixel to reach a defined threshold of its pre-disturbance NBR value. While the 80% threshold is commonly used, alternative thresholds have been proposed depending on how recovery is defined (White et al., 2018). Within C2C-GEE, Y2R can be evaluated at 60%, 80%, and 100% recovery thresholds (Table 2). Y2R depends on the pre-disturbance baseline, which in the C2C framework is defined as the average NBR over the two years preceding the disturbance (White, 2024; White et al., 2017). This metric has been applied to quantify forest recovery in a variety of environments, including the Pacific Northwest (Kennedy et al., 2012), Canada (Hird et al., 2021; White et al., 2017), Italy (Chirici et al., 2020), Australia (Nguyen et al., 2020), Borneo (Ioki et al., 2022), and Japan (Shimizu and Saito, 2021).

3.4. Opportunities for integration

The implementation of the C2C protocol on GEE extends the operational flexibility and accessibility of time series-based change detection and characterization. The availability of other well-established algorithms within the same platform (e.g., LandTrendr, BFAST, and CCDC) enables users to explore and compare various change detection approaches, as these methods differ in their segmentation philosophies, treatment of temporal trajectories, and their intended applications (Healey et al., 2018). For instance, LandTrendr emphasizes spectral trajectory segmentation and fitted vertex interpretation using annual observations (Kennedy et al., 2010); CCDC focuses on continuous harmonic modelling and iterative change monitoring using all available clear observations (Zhu and Woodcock, 2014); and BFAST uses dense time series observations to decompose temporal trajectories into trends and seasonal components to identify structural breaks (Verbesselt et al., 2010). C2C-GEE focuses on generating standardized disturbance and recovery metrics derived from piecewise spectral trajectories, with a particular focus on characterizing vegetation change and post-disturbance recovery dynamics. As such, these algorithms should not be expected to agree, but rather provide user options and complementary perspectives on the timing, intensity and nature of change events, expanding the information available for downstream applications (Zhu et al., 2022). The change metrics produced by C2C provide consistent, temporally informed inputs that can support a wide range of applications such as land cover classification (Griffiths et al., 2019; Hermosilla et al., 2022), biomass estimation (Liang et al., 2023; Matasci et al., 2018), and can also serve as inputs to predictive models for near-real-time or early warning systems (Ye et al., 2021a), particularly in contexts where the timing, magnitude, or duration of change are key factors (Kato et al., 2020; Pasquarella et al., 2017; Pelletier et al., 2024).

In addition to Landsat data, the C2C-GEE implementation can be applied to Sentinel-2 imagery or by integrating Landsat and Sentinel-2 observations using the HLS product (Ju et al., 2021; Radeloff et al., 2024). The increased frequency of observations provided by this virtual constellation of satellites reduces the impact of cloud cover and enhances the generation of seasonal composites and the analysis of within-year change metrics (Ju et al., 2025). This is particularly useful for capturing processes that occur on shorter timescales, such as phenological and agricultural cycles, which may be missed when relying solely on annual composites (Blickensdörfer et al., 2022; Bolton et al., 2020; Moon et al., 2021).

4. Conclusions

The C2C protocol characterizes change trajectories from dense optical time series data. The implementation of C2C on GEE provides access to temporal segmentation and metric extraction functions, enabling scalable generation of disturbance and recovery metrics without the need for local data storage or processing infrastructure. With access to the full Landsat archive and the option to integrate Sentinel-2 data, C2C-GEE supports monitoring of both abrupt and gradual land surface changes over large and ecologically diverse areas worldwide. The combination of temporal segmentation, noise filtering, change detection, and disturbance and recovery characterization enables the transparent and systematic generation of change metrics suitable for both mapping and modelling applications, ranging from forest disturbance mapping to post-disturbance regrowth monitoring and habitat assessment. The GEE environment allows transparent parameter tuning and algorithmic adaptation to local monitoring needs. This flexibility, together with the reproducibility of results and accessibility of globally representative data, provides a protocol for consistent long-term monitoring and supports further integration with modelling and decision-making frameworks.

Appendix

Software & code availability

The open-source Java code used to develop the GEE built-in C2C implementation is available at: https://github.com/saveriofrancini/C2C-GEE. A direct link[1] to the GEE Code Editor is also provided, allowing users to quickly visualize dynamically generated C2C-GEE outputs over European forest environments.

C2C-GEE is implemented as a native algorithm within the GEE platform and can be accessed through the GEE API (`ee.Algorithms.TemporalSegmentation.C2c`) using JavaScript or Python clients. Use of C2C-GEE requires a registered GEE account. The source code is distributed under the license specified in the repository.

CRediT authorship contribution statement

Txomin Hermosilla: Conceptualization, Methodology, Writing – original draft. **Michael A. Wulder:** Conceptualization, Writing – original draft. **Joanne C. White:** Conceptualization, Writing – original draft. **Nicholas C. Coops:** Conceptualization, Writing – original draft. **Daniel Coelho:** Software, Writing – original draft. **Giovanni Ciatto:** Software, Writing – original draft. **Noel Gorelick:** Software, Writing – original draft. **Emma Bambagioni:** Software, Validation. **Saverio Francini:** Conceptualization, Methodology, Software, Writing – original draft.

Declaration of competing interest

The authors declare that they have no known competing financial interests or personal relationships that could have appeared to influence the work reported in this paper.

Acknowledgments

Forest monitoring research and operationalization, including development of C2C, receives ongoing support from the Government of Canada. This study was also supported in part by the following projects: FORWARDS. H2020 project funded by the European Commission, number 101084481 call HORIZON-CL6-2022-CLIMATE-01-05 and NextGenCarbon, H2020 project funded by the European Commission, number 101184989 call HORIZON-CL5-2024-D1-01-07, and an NSERC Discovery grant to Coops. Open access supported by the Government of Canada.

[1] https://code.earthengine.google.com/f4ac48aea4ae9365f2e4a9a2133da3c6.

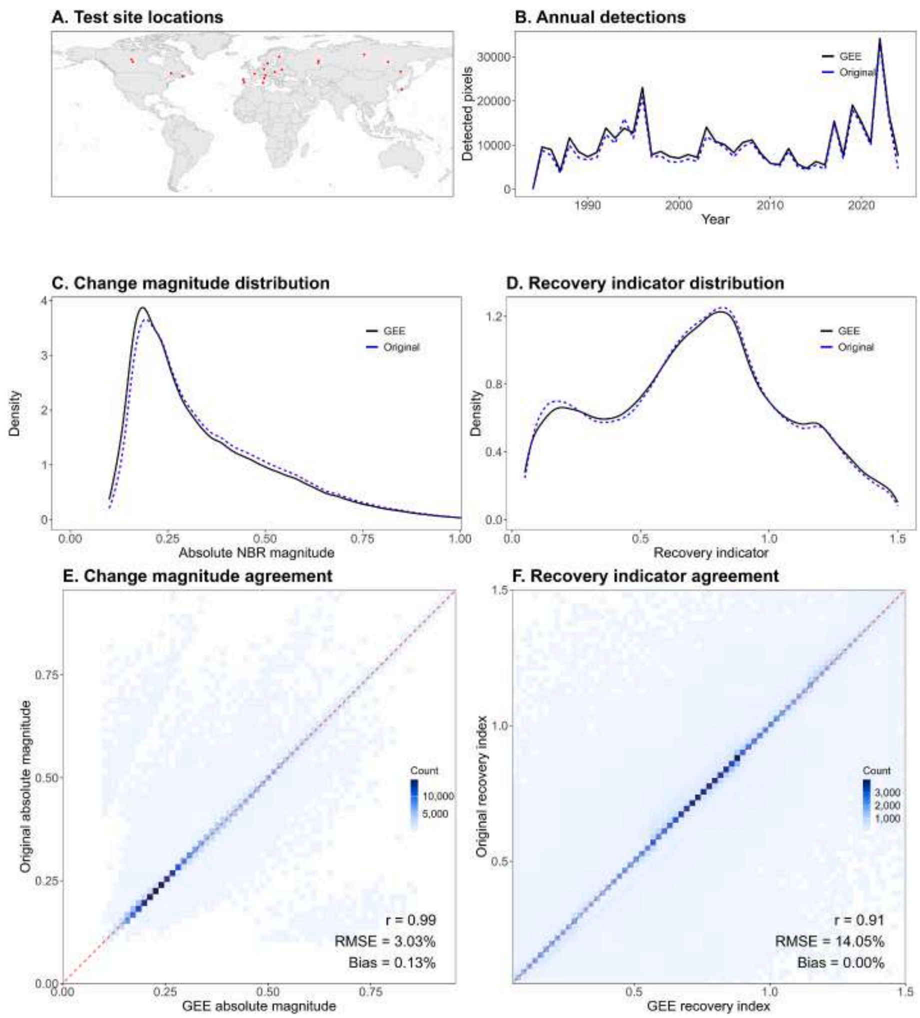

Fig. A1. Comparison of outputs generated by the Google Earth Engine implementation of Composite2Change (C2C-GEE) and the original local implementation using the same processing parameters across 21 northern hemisphere 5 × 5-km test sites. (A) Geographic distribution of test sites. (B) Annual disturbance detections aggregated across all sites. (C) Distribution of change magnitude. (D) Distribution of recovery indicator. (E) Agreement between implementations for disturbance magnitude. (F) Agreement between implementations for recovery indicator. Comparisons were restricted to forested pixels and disturbance detections exceeding a minimum magnitude (< -0.10) threshold.

Data availability

No data was used for the research described in the article.

References

Arévalo, P., Bullock, E.L., Woodcock, C.E., Olofsson, P., 2020. A suite of tools for continuous land change monitoring in Google Earth engine. Front. Clim. 2, 576740. https://doi.org/10.3389/fclim.2020.576740.

Baral, S.K., Boudewyn, P., Hermosilla, T., Fortin, M., White, J.C., Wulder, M.A., Schneider, R., Stinson, G., 2025. Improving sample-based National Forest Inventory estimates of tree cover using Landsat-derived land cover data as auxiliary information. Can. J. For. Res. 55, 1–19. https://doi.org/10.1139/cjfr-2024-0265.

Blickensdörfer, L., Schwieder, M., Pflugmacher, D., Nendel, C., Erasmi, S., Hostert, P., 2022. Mapping of crop types and crop sequences with combined time series of Sentinel-1, Sentinel-2 and Landsat 8 data for Germany. Remote Sens. Environ. 269, 112831. https://doi.org/10.1016/j.rse.2021.112831.

Bolton, D.K., Coops, N.C., Wulder, M.A., 2015. Characterizing residual structure and forest recovery following high-severity fire in the western boreal of Canada using Landsat time-series and airborne lidar data. Remote Sens. Environ. 163, 48–60. https://doi.org/10.1016/j.rse.2015.03.004.

Bolton, D.K., Gray, J.M., Melaas, E.K., Moon, M., Eklundh, L., Friedl, M.A., 2020. Continental-scale land surface phenology from harmonized Landsat 8 and Sentinel-2 imagery. Remote Sens. Environ. 240, 111685. https://doi.org/10.1016/j.rse.2020.111685.

Bright, B.C., Hudak, A.T., Kennedy, R.E., Braaten, J.D., Henareh Khalyani, A., 2019. Examining post-fire vegetation recovery with Landsat time series analysis in three western North American forest types. Fire Ecol. 15, 8. https://doi.org/10.1186/s42408-018-0021-9.

Brown, M.S., Coops, N.C., Mulverhill, C., Achim, A., 2025. Detection of non-stand replacing disturbances (NSR) using Harmonized Landsat-Sentinel-2 time series. ISPRS J. Photogrammetry Remote Sens. 220, 264–276. https://doi.org/10.1016/j.isprsjprs.2024.12.014.

Chen, Z., Chen, N., Yang, C., Di, L., 2012. Cloud computing enabled web processing service for earth observation data processing. IEEE J. Sel. Top. Appl. Earth Obs. Remote Sens. 5, 1637–1649. https://doi.org/10.1109/JSTARS.2012.2205372.

Chirici, G., Giannetti, F., Mazza, E., Francini, S., Travaglini, D., Pegna, R., White, J.C., 2020. Monitoring clearcutting and subsequent rapid recovery in Mediterranean coppice forests with Landsat time series. Ann. For. Sci 77. https://doi.org/10.1007/s13595-020-00936-2.

Chu, T., Guo, X., Takeda, K., 2017. Effects of burn severity and environmental conditions on post-fire regeneration in Siberian Larch forest. Forests 8, 76. https://doi.org/10.3390/f8030076.

Chu, T., Guo, X., 2013. Remote sensing techniques in monitoring post-fire effects and patterns of Forest recovery in boreal Forest regions: a review. Remote Sens. 6, 470–520. https://doi.org/10.3390/rs6010470.

Cohen, W., Healey, S., Yang, Z., Stehman, S., Brewer, C., Brooks, E., Gorelick, N., Huang, C., Hughes, M., Kennedy, R., Loveland, T., Moisen, G., Schroeder, T., Vogelmann, J., Woodcock, C., Yang, L., Zhu, Z., 2017. How similar are forest disturbance maps derived from different landsat time series algorithms? Forests 8, 98. https://doi.org/10.3390/f8040098.

Cohen, W.B., Healey, S.P., Yang, Z., Zhu, Z., Gorelick, N., 2020. Diversity of algorithm and spectral band inputs improves landsat monitoring of forest disturbance. Remote Sens. 12, 1–15. https://doi.org/10.3390/rs12101673.

Cohen, W.B., Yang, Z., Healey, S.P., Kennedy, R.E., Gorelick, N., 2018. A LandTrendr multispectral ensemble for forest disturbance detection. Remote Sens. Environ. 205, 131–140. https://doi.org/10.1016/j.rse.2017.11.015.

Cohen, W.B., Goward, S.N., 2004. Landsat's role in ecological applications of remote sensing. Bioscience 54, 535–545. https://doi.org/10.1641/0006-3568(2004)054[0535:LRIEAO]2.0.CO;2.

Comber, A., Wulder, M., 2019. Considering spatiotemporal processes in big data analysis: insights from remote sensing of land cover and land use. Trans. GIS 23, 879–891. https://doi.org/10.1111/tgis.12559.

Coops, N.C., Shang, C., Wulder, M.A., White, J.C., Hermosilla, T., 2020. Change in forest condition: characterizing non-stand replacing disturbances using time series satellite imagery. For. Ecol. Manage. 474, 118370. https://doi.org/10.1016/j.foreco.2020.118370.

Coops, N.C., Wulder, M.A., White, J.C., 2006. Identifying and describing forest disturbance and spatial pattern: data selection issues and methodological implications. In: Wulder, M.A., Franklin, S.E. (Eds.), Understanding Forest Disturbance and Spatial Pattern. CRC Press, New York, USA, pp. 31–61. https://doi.org/10.1201/9781420005189.ch2.

DeVries, B., Decuyper, M., Verbesselt, J., Zeileis, A., Herold, M., Joseph, S., 2015a. Tracking disturbance-regrowth dynamics in tropical forests using structural change detection and landsat time series. Remote Sens. Environ. 169, 320–334. https://doi.org/10.1016/j.rse.2015.08.020.

DeVries, B., Verbesselt, J., Kooistra, L., Herold, M., 2015b. Robust monitoring of small-scale forest disturbances in a tropical montane forest using Landsat time series. Remote Sens. Environ. 161, 107–121. https://doi.org/10.1016/j.rse.2015.02.012.

Esteban, J., Fernández-Landa, A., Tomé, J.L., Gómez, C., Marchamalo, M., 2021. Identification of silvicultural practices in mediterranean forests integrating landsat time series and a single coverage of als data. Remote Sens. 13. https://doi.org/10.3390/rs13183611.

Francini, S., 2022. BAP: best available pixel calculation using Google Earth Engine [WWW Document]. URL. https://github.com/saveriofrancini/bap (accessed 2.2.26).

Francini, S., Borghi, C., D'Amico, G., Waser, L.T., Lisiewicz, M., Stereńczak, K., Schelhaas, M.-J., Pellett, C., Gobakken, T., Næsset, E., Magnani, F., De-Miguel, S., Nabuurs, G.-J., Valbuena, R., Chirici, G., 2025. Bridging spatio-temporal gaps in ALS data using Landsat time series and forest disturbance-recovery metrics via multi-task neural networks. Sci. Remote Sens. 12, 100318. https://doi.org/10.1016/j.srs.2025.100318.

Francini, S., Hermosilla, T., Coops, N.C., Wulder, M.A., White, J.C., Chirici, G., 2023. An assessment approach for pixel-based image composites. ISPRS J. Photogrammetry Remote Sens. 202, 1–12. https://doi.org/10.1016/j.isprsjprs.2023.06.002.

Frazier, R.J., Coops, N.C., Wulder, M.A., Hermosilla, T., White, J.C., 2018. Analyzing spatial and temporal variability in short-term rates of post-fire vegetation return from Landsat time series. Remote Sens. Environ. 205, 32–45. https://doi.org/10.1016/j.rse.2017.11.007.

Frolking, S., Palace, M.W., Clark, D.B., Chambers, J.Q., Shugart, H.H., Hurtt, G.C., 2009. Forest disturbance and recovery: a general review in the context of spaceborne remote sensing of impacts on aboveground biomass and canopy structure. J. Geophys. Res. Biogeosci. 114, G00E02. https://doi.org/10.1029/2008JG000911.

Fu, Y., Li, J., Weng, Q., Zheng, Q., Li, L., Dai, S., Guo, B., 2019. Characterizing the spatial pattern of annual urban growth by using time series Landsat imagery. Sci. Total Environ. 666, 274–284. https://doi.org/10.1016/j.scitotenv.2019.02.178.

Giambelluca, A.L., Hermosilla, T., Álvarez-Mozos, J., González-Audícana, M., 2025. Identifying forest harvesting practices: Clear-cutting and thinning in diverse tree species using dense Landsat time series. For. Ecol. Manage. 578, 122442. https://doi.org/10.1016/j.foreco.2024.122442.

Gorelick, N., Hancher, M., Dixon, M., Ilyushchenko, S., Thau, D., Moore, R., 2017. Google Earth Engine: Planetary-scale geospatial analysis for everyone. Remote Sens. Environ. 202, 18–27. https://doi.org/10.1016/j.rse.2017.06.031.

Griffiths, P., Kuemmerle, T., Baumann, M., Radeloff, V.C., Abrudan, I.V., Lieskovsky, J., Munteanu, C., Ostapowicz, K., Hostert, P., 2014. Forest disturbances, forest recovery, and changes in forest types across the Carpathian ecoregion from 1985 to 2010 based on Landsat image composites. Remote Sens. Environ. 151, 72–88. https://doi.org/10.1016/j.rse.2013.04.022.

Griffiths, P., Nendel, C., Hostert, P., 2019. Intra-annual reflectance composites from Sentinel-2 and Landsat for national-scale crop and land cover mapping. Remote Sens. Environ. 220, 135–151. https://doi.org/10.1016/j.rse.2018.10.031.

Griffiths, P., van der Linden, S., Kuemmerle, T., Hostert, P., 2013. A pixel-based landsat compositing Algorithm for large area land cover mapping. IEEE J. Sel. Top. Appl. Earth Obs. Remote Sens. 6, 2088–2101. https://doi.org/10.1109/JSTARS.2012.2228167.

Hais, M., Wild, J., Berec, L., Brůna, J., Kennedy, R., Braaten, J., Brož, Z., 2016. Landsat imagery spectral trajectories-important variables for spatially predicting the risks of bark beetle disturbance. Remote Sens. 8, 687. https://doi.org/10.3390/rs8080687.

Hamunyela, E., Rosca, S., Mirt, A., Engle, E., Herold, M., Gieseke, F., Verbesselt, J., 2020. Implementation of BFASTmonitor algorithm on Google Earth engine to support large-area and sub-annual change monitoring using Earth observation data. Remote Sens. 12, 2953. https://doi.org/10.3390/rs12182953.

Hansen, M.C., Potapov, P.V., Moore, R., Hancher, M., Turubanova, S.A., Tyukavina, A., Thau, D., Stehman, S.V., Goetz, S.J., Loveland, T.R., Kommareddy, A., Egorov, A., Chini, L., Justice, C.O., Townshend, J.R.G., 2013. High-resolution global maps of 21st-century forest cover change. Science 342, 850–853. https://doi.org/10.1126/science.1244693.

Hansen, M.C., Loveland, T.R., 2012. A review of large area monitoring of land cover change using Landsat data. Remote Sens. Environ. 122, 66–74. https://doi.org/10.1016/j.rse.2011.08.024.

Healey, S.P., Cohen, W.B., Yang, Z., Kenneth Brewer, C., Brooks, E.B., Gorelick, N., Hernandez, A.J., Huang, C., Joseph Hughes, M., Kennedy, R.E., Loveland, T.R., Moisen, G.G., Schroeder, T.A., Stehman, S.V., Vogelmann, J.E., Woodcock, C.E., Yang, L., Zhu, Z., 2018. Mapping forest change using stacked generalization: an ensemble approach. Remote Sens. Environ. 204, 717–728. https://doi.org/10.1016/j.rse.2017.09.029.

Hermosilla, T., Francini, S., Nicolau, A.P., Wulder, M.A., White, J.C., Coops, N.C., Chirici, G., 2024a. Clouds and image compositing. In: Cardille, J.A., Crowley, M.A., Saah, D., Clinton, N.E. (Eds.), Cloud-Based Remote Sensing with Google Earth Engine. Springer International Publishing, Cham, pp. 279–302. https://doi.org/10.1007/978-3-031-26588-4_15.

Hermosilla, T., Wulder, M.A., White, J.C., Coops, N.C., 2019. Prevalence of multiple forest disturbances and impact on vegetation regrowth from interannual Landsat time series (1985–2015). Remote Sens. Environ. 233, 111403. https://doi.org/10.1016/j.rse.2019.111403.

Hermosilla, T., Wulder, M.A., White, J.C., Coops, N.C., 2022. Land cover classification in an era of big and open data: optimizing localized implementation and training data selection to improve mapping outcomes. Remote Sens. Environ. 268, 112780. https://doi.org/10.1016/j.rse.2021.112780.

Hermosilla, T., Wulder, M.A., White, J.C., Coops, N.C., Bater, C.W., Hobart, G.W., 2024b. Characterizing long-term tree species dynamics in Canada's forested ecosystems using annual time series remote sensing data. For. Ecol. Manage. 572, 122313. https://doi.org/10.1016/j.foreco.2024.122313.

Hermosilla, T., Wulder, M.A., White, J.C., Coops, N.C., Hobart, G.W., 2015a. An integrated Landsat time series protocol for change detection and generation of annual gap-free surface reflectance composites. Remote Sens. Environ. 158, 220–234. https://doi.org/10.1016/j.rse.2014.11.005.

Hermosilla, T., Wulder, M.A., White, J.C., Coops, N.C., Hobart, G.W., 2015b. Regional detection, characterization, and attribution of annual forest change from 1984 to 2012 using Landsat-derived time-series metrics. Remote Sens. Environ. 170, 121–132. https://doi.org/10.1016/j.rse.2015.09.004.

Hermosilla, T., Wulder, M.A., White, J.C., Coops, N.C., Hobart, G.W., 2018. Disturbance-informed annual land cover classification maps of Canada's forested ecosystems for a 29-Year landsat time series. Can. J. Rem. Sens. 44, 67–87. https://doi.org/10.1080/07038992.2018.1437719.

Hermosilla, T., Wulder, M.A., White, J.C., Coops, N.C., Hobart, G.W., Campbell, L.B., 2016. Mass data processing of time series Landsat imagery: pixels to data products for forest monitoring. Int. J. Digit. Earth 9, 1035–1054. https://doi.org/10.1080/17538947.2016.1187673.

Hilker, T., 2011. Biweekly disturbance capture and attribution: case study in western Alberta grizzly bear habitat. J. Appl. Remote Sens. 5, 053568. https://doi.org/10.1117/1.3664342.

Hird, J.N., Kariyeva, J., McDermid, G.J., 2021. Satellite time series and google earth engine democratize the process of forest-recovery monitoring over large areas. Remote Sens. 13. https://doi.org/10.3390/rs13234745.

Hughes, M., Kaylor, S., Hayes, D., 2017. Patch-Based Forest change detection from landsat time series. Forests 8, 166. https://doi.org/10.3390/f8050166.

Ioki, K., James, D., Phua, M.H., Tsuyuki, S., Imai, N., 2022. Recovery of tree community composition across different types of anthropogenic disturbances and characterization of their effect using Landsat time series in Bornean tropical montane forest. Biol. Conserv. 267, 109489. https://doi.org/10.1016/j.biocon.2022.109489.

Jarron, L.R., Hermosilla, T., Coops, N.C., Wulder, M.A., White, J.C., Hobart, G.W., Leckie, D.G., 2017. Differentiation of alternate harvesting practices using annual time series of landsat data. Forests 8. https://doi.org/10.3390/f8010015.

Ju, J., Neigh, C., Claverie, M., Skakun, S., Roger, J.-C., Vermote, E., Dungan, J., 2021. Harmonized Landsat-8 Sentinel-2 (HLS) product user's guide. Product Version 2.0. National Aeronautics and Space Administration, Goddard Space Flight Center, Greenbelt, Maryland, USA. https://lpdaac.usgs.gov/documents/1698/HLS_User_Guide_V2.pdf.

Ju, J., Zhou, Q., Freitag, B., Roy, D.P., Zhang, H.K., Sridhar, M., Mandel, J., Arab, S., Schmidt, G., Crawford, C.J., Gascon, F., Strobl, P.A., Masek, J.G., Neigh, C.S.R., 2025. The harmonized landsat and Sentinel-2 version 2.0 surface reflectance dataset. Remote Sens. Environ. 324, 114723. https://doi.org/10.1016/j.rse.2025.114723.

Kato, A., Thau, D., Hudak, A.T., Meigs, G.W., Moskal, L.M., 2020. Quantifying fire trends in boreal forests with Landsat time series and self-organized criticality. Remote Sens. Environ. 237, 111525. https://doi.org/10.1016/j.rse.2019.111525.

Kearney, S.P., Coops, N.C., Stenhouse, G.B., Nielsen, S.E., Hermosilla, T., White, J.C., Wulder, M.A., 2019. Grizzly bear selection of recently harvested forests is dependent on forest recovery rate and landscape composition. For. Ecol. Manage. 449, 117459. https://doi.org/10.1016/j.foreco.2019.117459.

Kennedy, R., Yang, Z., Gorelick, N., Braaten, J., Cavalcante, L., Cohen, W., Healey, S., 2018. Implementation of the LandTrendr algorithm on Google Earth engine. Remote Sens. 10, 691. https://doi.org/10.3390/rs10050691.

Kennedy, R.E., Yang, Z., Braaten, J., Copass, C., Antonova, N., Jordan, C., Nelson, P., 2015. Attribution of disturbance change agent from Landsat time-series in support of habitat monitoring in the Puget Sound region, USA. Remote Sens. Environ. 166, 271–285. https://doi.org/10.1016/j.rse.2015.05.005.

Kennedy, R.E., Yang, Z., Cohen, W.B., 2010. Detecting trends in forest disturbance and recovery using yearly Landsat time series: 1. LandTrendr - temporal segmentation algorithms. Remote Sens. Environ. 114, 2897–2910. https://doi.org/10.1016/j.rse.2010.07.008.

Kennedy, R.E., Yang, Z., Cohen, W.B., Pfaff, E., Braaten, J., Nelson, P., 2012. Spatial and temporal patterns of forest disturbance and regrowth within the area of the Northwest Forest Plan. Remote Sens. Environ. 122, 117–133. https://doi.org/10.1016/j.rse.2011.09.024.

Keogh, E., Chu, S., Hart, D., Pazzani, M., 2001. An online algorithm for segmenting time series. In: Proceedings 2001 IEEE International Conference on Data Mining. IEEE Comput. Soc, San Jose, CA, pp. 289–296. https://doi.org/10.1109/ICDM.2001.989531.

Key, C.H., Benson, N.C., 2006. Landscape assessment: sampling and analysis methods. In: Lutes, D.C., Keane, R.E., Caratti, J.F., Key, C.H., Benson, N.C., Sutherland, S., Gangi, L.J. (Eds.), FIREMON: Fire Effects Monitoring and Inventory System. Department of Agriculture, Forest Service, Rocky Mountain Research Station, Fort Collins, CO: U.S.

Liang, M., Duncanson, L., Silva, J.A., Sedano, F., 2023. Quantifying aboveground biomass dynamics from charcoal degradation in Mozambique using GEDI Lidar and Landsat. Remote Sens. Environ. 284, 113367. https://doi.org/10.1016/j.rse.2022.113367.

Mandl, L., Cerioni, M., Bače, R., Bončina, A., Brůna, J., Chećko, E., de Koning, J.H.C., Diaci, J., Dobrowolska, D., Fidej, G., Garbarino, M., Jansons, Ā., Keren, S., Kitenberga, M., Klopčič, M., Konôpka, B., Kopecký, M., Köster, K., Kucbel, S., Lingua, E., Macek, M., Marzano, R., Metslaid, M., Panayotov, M., Pittner, J., Šebeň, V., Socha, J., Svoboda, M., Szwagrzyk, J., Tsvetanov, N., Urbinati, C., Vencurik, J., Vitali, A., Vodde, F., Wild, J., Nagel, T.A., Senf, C., 2025. The amount of undisturbed forest in proximity of severe disturbance patches enhances their recovery in temperate Europe. Landsc. Ecol. 40, 199. https://doi.org/10.1007/s10980-025-02231-9.

Masek, J.G., Vermote, E.F., Saleous, N.E., Wolfe, R., Hall, F.G., Huemmrich, K.F., Gao, F., Kutler, J., Lim, T.K., 2006. A landsat surface reflectance dataset for North America, 1990-2000. IEEE Geosci. Remote Sens. Lett. 3, 68–72. https://doi.org/10.1109/LGRS.2005.857030.

Matasci, G., Hermosilla, T., Wulder, M.A., White, J.C., Coops, N.C., Hobart, G.W., Bolton, D.K., Tompalski, P., Bater, C.W., 2018. Three decades of forest structural dynamics over Canada's forested ecosystems using Landsat time-series and lidar plots. Remote Sens. Environ. 216, 697–714. https://doi.org/10.1016/j.rse.2018.07.024.

Meigs, G.W., Kennedy, R.E., Cohen, W.B., 2011. A Landsat time series approach to characterize bark beetle and defoliator impacts on tree mortality and surface fuels in conifer forests. Remote Sens. Environ. 115, 3707–3718. https://doi.org/10.1016/j.rse.2011.09.009.

Meng, X., Xie, S., Sun, L., Liu, L., Han, Y., 2023. Evaluation of temporal compositing algorithms for annual land cover classification using Landsat time series data. Int. J. Digit. Earth 16, 2574–2598. https://doi.org/10.1080/17538947.2023.2230958.

Moon, M., Richardson, A.D., Friedl, M.A., 2021. Multiscale assessment of land surface phenology from harmonized Landsat 8 and Sentinel-2, PlanetScope, and PhenoCam imagery. Remote Sens. Environ. 266, 112716. https://doi.org/10.1016/j.rse.2021.112716.

Mulverhill, C., Coops, N.C., Wulder, M.A., White, J.C., Hermosilla, T., Bater, C.W., 2024. Multidecadal mapping of status and trends in annual burn probability over Canada's forested ecosystems. ISPRS J. Photogrammetry Remote Sens. 209, 279–295. https://doi.org/10.1016/j.isprsjprs.2024.02.006.

Nguyen, T.H., Jones, S.D., Soto-Berelov, M., Haywood, A., Hislop, S., 2020. Monitoring aboveground forest biomass dynamics over three decades using Landsat time-series and single-date inventory data. Int. J. Appl. Earth Obs. Geoinf. 84, 101952. https://doi.org/10.1016/j.jag.2019.101952.

Pasquarella, V., Bradley, B., Woodcock, C., 2017. Near-Real-Time monitoring of insect defoliation using landsat time series. Forests 8, 275. https://doi.org/10.3390/f8080275.

Pasquarella, V.J., Mickley, J.G., Barker Plotkin, A., MacLean, R.G., Anderson, R.M., Brown, L.M., Wagner, D.L., Singer, M.S., Bagchi, R., 2021. Predicting defoliator abundance and defoliation measurements using Landsat-based condition scores. Remote Sens. Ecol. Conserv. 7, 592–609. https://doi.org/10.1002/rse2.211.

Pelletier, F., Cardille, J.A., Wulder, M.A., White, J.C., Hermosilla, T., 2024. Revisiting the 2023 wildfire season in Canada. Sci. Remote Sens. 10, 100145. https://doi.org/10.1016/j.srs.2024.100145.

Pflugmacher, D., Cohen, W.B., Kennedy, R.E., Yang, Z., 2014. Using landsat-derived disturbance and recovery history and lidar to map forest biomass dynamics. Remote Sens. Environ. 151, 124–137. https://doi.org/10.1016/j.rse.2013.05.033.

Pickell, P.D., Hermosilla, T., Coops, N.C., Masek, J.G., Franks, S., Huang, C., 2014. Monitoring anthropogenic disturbance trends in an industrialized boreal forest with Landsat time series. Remote Sens. Lett 5, 783–792. https://doi.org/10.1080/2150704X.2014.967881.

Pickell, P.D., Hermosilla, T., Frazier, R.J., Coops, N.C., Wulder, M.A., 2016. Forest recovery trends derived from Landsat time series for North American boreal forests. Int. J. Rem. Sens. 37, 138–149. https://doi.org/10.1080/2150704X.2015.1126375.

Potapov, P.V., Turubanova, S.A., Tyukavina, A., Krylov, A.M., McCarty, J.L., Radeloff, V.C., Hansen, M.C., 2015. Eastern Europe's forest cover dynamics from 1985 to 2012 quantified from the full Landsat archive. Remote Sens. Environ. 159, 28–43. https://doi.org/10.1016/j.rse.2014.11.027.

Pouliot, D., Latifovic, R., 2016. Land change attribution based on Landsat time series and integration of ancillary disturbance data in the Athabasca oil sands region of Canada. GIScience Remote Sens. 53, 382–401. https://doi.org/10.1080/15481603.2015.1137112.

Pugh, T.A.M., Lindeskog, M., Smith, B., Poulter, B., Arneth, A., Haverd, V., Calle, L., 2019. Role of forest regrowth in global carbon sink dynamics. Proc. Natl. Acad. Sci. U. S. A. 116, 4382–4387. https://doi.org/10.1073/pnas.1810512116.

Qiu, S., Zhu, Z., Olofsson, P., Woodcock, C.E., Jin, S., 2023. Evaluation of Landsat image compositing algorithms. Remote Sens. Environ. 285, 113375. https://doi.org/10.1016/j.rse.2022.113375.

Radeloff, V.C., Roy, D.P., Wulder, M.A., Anderson, M., Cook, B., Crawford, C.J., Friedl, M., Gao, F., Gorelick, N., Hansen, M., Healey, S., Hostert, P., Hulley, G., Huntington, J.L., Johnson, D.M., Neigh, C., Lyapustin, A., Lymburner, L., Pahlevan, N., Pekel, J.-F., Scambos, T.A., Schaaf, C., Strobl, P., Woodcock, C.E., Zhang, H.K., Zhu, Z., 2024. Need and vision for global medium-resolution Landsat and Sentinel-2 data products. Remote Sens. Environ. 300, 113918. https://doi.org/10.1016/j.rse.2023.113918.

Rickbeil, G.J.M., Hermosilla, T., Coops, N.C., White, J.C., Wulder, M.A., 2017. Barren-ground caribou (Rangifer tarandus groenlandicus) behaviour after recent fire events; integrating caribou telemetry data with Landsat fire detection techniques. Glob. Change Biol. 23, 1036–1047. https://doi.org/10.1111/gcb.13456.

Roy, D.P., Ju, J., Kline, K., Scaramuzza, P.L., Kovalskyy, V., Hansen, M., Loveland, T.R., Vermote, E., Zhang, C., 2010. Web-enabled Landsat Data (WELD): Landsat ETM+ composited mosaics of the conterminous United States. Remote Sens. Environ. 114, 35–49. https://doi.org/10.1016/j.rse.2009.08.011.

Schleeweis, K.G., Moisen, G.G., Schroeder, T.A., Toney, C., Freeman, E.A., Goward, S.N., Huang, C., Dungan, J.L., 2020. US national maps attributing Forest change: 1986–2010. Forests 11, 653. https://doi.org/10.3390/f11060653.

Schmidt, G., Jenkerson, C., Masek, J., Vermote, E., Gao, F., 2013. Landsat ecosystem disturbance adaptive processing system (LEDAPS) algorithm description. Reston, VA. https://doi.org/10.3133/ofr20131057.

Schroeder, T.A., Cohen, W.B., Yang, Z., 2007. Patterns of forest regrowth following clearcutting in western Oregon as determined from a Landsat time-series. For. Ecol. Manage. 243, 259–273. https://doi.org/10.1016/j.foreco.2007.03.019.

Schroeder, T.A., Healey, S.P., Moisen, G.G., Frescino, T.S., Cohen, W.B., Huang, C., Kennedy, R.E., Yang, Z., 2014. Improving estimates of forest disturbance by combining observations from landsat time series with U.S. Forest Service Forest Inventory and Analysis data. Remote Sens. Environ. 154, 61–73. https://doi.org/10.1016/j.rse.2014.08.005.

Schroeder, T.A., Schleeweis, K.G., Moisen, G.G., Toney, C., Cohen, W.B., Freeman, E.A., Yang, Z., Huang, C., 2017. Testing a Landsat-based approach for mapping disturbance causality in U.S. forests. Remote Sens. Environ. 195, 230–243. https://doi.org/10.1016/j.rse.2017.03.033.

Sebald, J., Senf, C., Seidl, R., 2021. Human or natural? Landscape context improves the attribution of forest disturbances mapped from Landsat in Central Europe. Remote Sens. Environ. 262, 112502. https://doi.org/10.1016/j.rse.2021.112502.

Senf, C., Pflugmacher, D., Wulder, M.A., Hostert, P., 2015. Characterizing spectral-temporal patterns of defoliator and bark beetle disturbances using Landsat time series. Remote Sens. Environ. 170, 166–177. https://doi.org/10.1016/j.rse.2015.09.019.

Senf, C., Seidl, R., Hostert, P., 2017. Remote sensing of forest insect disturbances: current state and future directions. Int. J. Appl. Earth Obs. Geoinf. 60, 49–60. https://doi.org/10.1016/j.jag.2017.04.004.

Senf, C., Seidl, R., 2022. Post-disturbance canopy recovery and the resilience of Europe's forests. Global Ecol. Biogeogr. 31, 25–36. https://doi.org/10.1111/geb.13406.

Shang, C., Wulder, M.A., Coops, N.C., White, J.C., 2020. Spatially-Explicit prediction of wildfire burn probability using remotely-sensed and ancillary data. Can. J. Rem. Sens. 1–17. https://doi.org/10.1080/07038992.2020.1788385.

Shimizu, K., Ahmed, O.S., Ponce-Hernandez, R., Ota, T., Win, Z.C., Mizoue, N., Yoshida, S., 2017. Attribution of disturbance agents to forest change using a landsat time series in tropical seasonal forests in the Bago Mountains, Myanmar. Forests 8, 218. https://doi.org/10.3390/f8060218.

Shimizu, K., Saito, H., 2021. Country-wide mapping of harvest areas and post-harvest forest recovery using Landsat time series data in Japan. Int. J. Appl. Earth Obs. Geoinf. 104, 102555. https://doi.org/10.1016/j.jag.2021.102555.

Smith-Tripp, S.M., Coops, N.C., Meyer, J., White, J.C., Gergel, S., Axelson, J., Roeser, D., 2026. Synthesizing spectral and field observations of post-fire conifer recovery in dry conifer forests. Ecosystems 29, 11. https://doi.org/10.1007/s10021-025-01029-9.

Smith-Tripp, S.M., Coops, N.C., Mulverhill, C., White, J.C., Axelson, J., 2024. Landsat assessment of variable spectral recovery linked to post-fire forest structure in dry sub-boreal forests. ISPRS J. Photogrammetry Remote Sens. 208, 121–135. https://doi.org/10.1016/j.isprsjprs.2024.01.008.

Smith-Tripp, S., Coops, N.C., Mulverhill, C., White, J.C., Gergel, S., 2025. Early spectral dynamics are indicative of distinct growth patterns in post-wildfire forests. Remote Sens. Ecol. Conserv. 11, 221–238. https://doi.org/10.1002/rse2.420.

Smyth, C., Fellows, M., Morken, S., Magnan, M., 2024. Development of national post-fire restoration system to assess net GHG impacts and salvage biomass availability. MethodsX 13, 102932. https://doi.org/10.1016/j.mex.2024.102932.

Song, X.P., Sexton, J.O., Huang, C., Channan, S., Townshend, J.R., 2016. Characterizing the magnitude, timing and duration of urban growth from time series of Landsat-based estimates of impervious cover. Remote Sens. Environ. 175, 1–13. https://doi.org/10.1016/j.rse.2015.12.027.

Stahl, A.T., Andrus, R., Hicke, J.A., Hudak, A.T., Bright, B.C., Meddens, A.J.H., 2023. Automated attribution of forest disturbance types from remote sensing data: a synthesis. Remote Sens. Environ. 285, 113416. https://doi.org/10.1016/j.rse.2022.113416.

Stewart, B.P., Wulder, M.A., McDermid, G.J., Nelson, T., 2009. Disturbance capture and attribution through the integration of Landsat and IRS-1C imagery. Can. J. Rem. Sens. 35, 523–533. https://doi.org/10.5589/m10-006.

Thapa, B., Wolter, P.T., Sturtevant, B.R., Townsend, P.A., 2022. Linking remote sensing and insect defoliation biology – a cross-system comparison. Remote Sens. Environ. 281, 113236. https://doi.org/10.1016/j.rse.2022.113236.

Tortini, R., Mayer, A.L., Hermosilla, T., Coops, N.C., Wulder, M.A., 2019. Using annual Landsat imagery to identify harvesting over a range of intensities for non-industrial family forests. Landsc. Urban Plann. 188, 143–150. https://doi.org/10.1016/j.landurbplan.2018.04.012.

Verbesselt, J., Hyndman, R., Newnham, G., Culvenor, D., 2010. Detecting trend and seasonal changes in satellite image time series. Remote Sens. Environ. 114, 106–115. https://doi.org/10.1016/j.rse.2009.08.014.

Vogeler, J.C., Slesak, R.A., Fekety, P.A., Falkowski, M.J., 2020. Characterizing over four decades of forest disturbance in minnesota, USA. Forests 11, 1–18. https://doi.org/10.3390/F11030362.

Vogeler, J.C., Yang, Z., Cohen, W.B., 2016. Mapping post-fire habitat characteristics through the fusion of remote sensing tools. Remote Sens. Environ. 173, 294–303. https://doi.org/10.1016/j.rse.2015.08.011.

Vogelmann, J.E., Gallant, A.L., Shi, H., Zhu, Z., 2016. Perspectives on monitoring gradual change across the continuity of Landsat sensors using time-series data. Remote Sens. Environ. 185, 258–270. https://doi.org/10.1016/j.rse.2016.02.060.

Vogelmann, J.E., Xian, G., Homer, C., Tolk, B., 2012. Monitoring gradual ecosystem change using Landsat time series analyses: case studies in selected forest and rangeland ecosystems. Remote Sens. Environ. 122, 92–105. https://doi.org/10.1016/j.rse.2011.06.027.

White, J.C., 2024. Characterizing forest recovery following stand-replacing disturbances in boreal forests: contributions of optical time series and airborne laser scanning data. Silva Fenn. 58, 23076. https://doi.org/10.14214/sf.23076.

White, J.C., Hermosilla, T., Wulder, M.A., Coops, N.C., 2022. Mapping, validating, and interpreting spatio-temporal trends in post-disturbance forest recovery. Remote Sens. Environ. 271, 112904. https://doi.org/10.1016/j.rse.2022.112904.

White, J.C., Saarinen, N., Kankare, V., Wulder, M.A., Hermosilla, T., Coops, N.C., Pickell, P.D., Holopainen, M., Hyyppä, J., Vastaranta, M., 2018. Confirmation of post-harvest spectral recovery from Landsat time series using measures of forest cover and height derived from airborne laser scanning data. Remote Sens. Environ. 216, 262–275. https://doi.org/10.1016/j.rse.2018.07.004.

White, J.C., Saarinen, N., Wulder, M.A., Kankare, V., Hermosilla, T., Coops, N.C., Holopainen, M., Hyyppä, J., Vastaranta, M., 2019. Assessing spectral measures of post-harvest forest recovery with field plot data. Int. J. Appl. Earth Obs. Geoinf. 80, 102–114. https://doi.org/10.1016/j.jag.2019.04.010.

White, J.C., Wulder, M.A., Hermosilla, T., Coops, N.C., Hobart, G.W., 2017. A nationwide annual characterization of 25 years of forest disturbance and recovery for Canada using Landsat time series. Remote Sens. Environ. 194, 303–321. https://doi.org/10.1016/j.rse.2017.03.035.

White, J.C., Wulder, M.A., Hobart, G.W., Luther, J.E., Hermosilla, T., Griffiths, P., Coops, N.C., Hall, R.J., Hostert, P., Dyk, A., Guindon, L., 2014. Pixel-based image compositing for large-area dense time series applications and science. Can. J. Rem. Sens. 40, 192–212. https://doi.org/10.1080/07038992.2014.945827.

White, J.C., Wulder, M.A., 2014. The Landsat observation record of Canada: 1972–2012. Can. J. Rem. Sens. 39, 455–467. https://doi.org/10.5589/m13-053.

Woodcock, C.E., Loveland, T.R., Herold, M., Bauer, M.E., 2020. Transitioning from change detection to monitoring with remote sensing: a paradigm shift. Remote Sens. Environ. 238, 111558. https://doi.org/10.1016/j.rse.2019.111558.

Wulder, M.A., White, J.C., Loveland, T.R., Woodcock, C.E., Belward, A.S., Cohen, W.B., Fosnight, E.A., Shaw, J., Masek, J.G., Roy, D.P., 2016. The global Landsat archive: status, consolidation, and direction. Remote Sens. Environ. 185, 271–283. https://doi.org/10.1016/j.rse.2015.11.032.

Wulder, M.A., Coops, N.C., 2014. Satellites: make Earth observations open access. Nature 513, 30–31. https://doi.org/10.1038/513030a.

Ye, S., Rogan, J., Zhu, Z., Eastman, J.R., 2021a. A near-real-time approach for monitoring forest disturbance using Landsat time series: stochastic continuous change detection. Remote Sens. Environ. 252, 112167. https://doi.org/10.1016/j.rse.2020.112167.

Ye, S., Rogan, J., Zhu, Z., Hawbaker, T.J., Hart, S.J., Andrus, R.A., Meddens, A.J.H., Hicke, J.A., Eastman, J.R., Kulakowski, D., 2021b. Detecting subtle change from dense Landsat time series: case studies of mountain pine beetle and spruce beetle disturbance. Remote Sens. Environ. 263, 112560. https://doi.org/10.1016/j.rse.2021.112560.

Zha, Y., Gao, J., Ni, S., 2003. Use of normalized difference built-up index in automatically mapping urban areas from TM imagery. Int. J. Rem. Sens. 24, 583–594. https://doi.org/10.1080/01431160304987.

Zhang, Y., Woodcock, C.E., Chen, S., Wang, J.A., Sulla-Menashe, D., Zuo, Z., Olofsson, P., Wang, Y., Friedl, M.A., 2022. Mapping causal agents of disturbance in boreal and arctic ecosystems of North America using time series of Landsat data. Remote Sens. Environ. 272, 112935. https://doi.org/10.1016/j.rse.2022.112935.

Zhu, Z., 2017. Change detection using landsat time series: a review of frequencies, preprocessing, algorithms, and applications. ISPRS J. Photogrammetry Remote Sens. 130, 370–384. https://doi.org/10.1016/j.isprsjprs.2017.06.013.

Zhu, Z., Qiu, S., Ye, S., 2022. Remote sensing of land change: a multifaceted perspective. Remote Sens. Environ. 282, 113266. https://doi.org/10.1016/j.rse.2022.113266.

Zhu, Z., Woodcock, C.E., 2014. Continuous change detection and classification of land cover using all available Landsat data. Remote Sens. Environ. 144, 152–171. https://doi.org/10.1016/j.rse.2014.01.011.